Chapter 8
The 34-Meter Beam-Waveguide Operational Antennas

With the successful completion of the Deep Space Station 13 (DSS-13) research and development (R&D) beam-waveguide (BWG) antenna, the decision was made to introduce 34-m BWG antennas into the operational network. The initial plan was to build three 34-m antennas at each of the Deep Space Network (DSN) complexes (Australia, Spain, and the U.S.). Arraying the three 34-m BWG antennas with the already existing 34-m high-efficiency (HEF) antenna would provide a *G/T* capability similar to that of the 70-m antenna and could, therefore, serve as a backup to the DSN's aging 70-m antennas. Due to funding constraints, however, three antennas (DSS-24, DSS-25, and DSS-26) were built at the Goldstone, California, complex, but only one antenna at each of the overseas complexes. Currently, a second BWG antenna is under construction in Spain.

8.1 Beam-Waveguide Design

The initial design was for simultaneous S-band (2.270–2.3 GHz receive and 2.110–2.120 GHz transmit) and X-band (8.4–8.5 GHz receive and 7.145–7.190 GHz transmit) operation, although the back structure, main reflector panels, subreflector, and BWG mirrors were to be designed and manufactured accurately enough to permit Ka-band (31.8–32.2 GHz receive and 34.2–43.7 GHz transmit) operation. At the time that the antenna was being designed, only Phase I (X- and Ka-band operation) of the R&D antenna had been completed, and the low-frequency problem had been identified but not yet

solved using the focal plane method [1]. Consequently, another design technique was used.

While geometrical optics (GO) was useful for designing high-frequency or electrically large mirrors (>50 wavelengths in diameter with 20-dB edge taper), this BWG needed to be operated at low frequencies, where the mirrors are as small as 20 wavelengths in diameter. Due to diffraction effects, the characteristics of a field propagated between small BWG mirrors (<30 wavelengths in diameter) are substantially different from the GO solution [2]. For these cases, the Gaussian beam technique can be utilized.

Gaussian-beam modes are an approximate solution of the wave equation describing a beam of radiation that is unguided but effectively confined near an optical axis. The zero-order mode is normally used in the design. A major advantage of the Gaussian technique is the simplicity of the Gaussian formula, which is easy to implement and requires negligible computation time.

Because of the short computation time, a Gaussian solution can be incorporated with an optimization routine to provide a convenient method to search design parameters for a specified frequency range, mirror sizes and locations, and horn parameters.

Although Gaussian-beam analysis is fast and simple, it is less accurate than the physical optics (PO) solution for smaller mirrors (<30 wavelengths in diameter). Further comparisons between Gaussian-beam techniques and PO analysis can be found in [3] and [4]. However, by designing with Gaussian beam analysis and checking and adjusting using PO analysis, an accurate and efficient tool can be fashioned. Veruttipong [5] developed such a tool for designing the operational 34-m BWG antenna for the DSN. The goal was to provide performance over the range of 2–32 GHz.

The design is similar to that of the DSS-13 antenna in that it uses three curved mirrors (one in the basement room and two rotating in azimuth) and a 34-m dual-shaped reflector antenna (Fig. 8-1). Multiple frequency operation is provided by the use of dichroic mirrors or multiple frequency feeds. The desire is to have the radius of curvature (i.e., phase center location) and –18-dB beam diameter of the Gaussian beam at the subreflector be the same at all frequencies. The size and locations of the mirrors are relatively fixed because of the basic structure geometry, so the pertinent variables are the feed-horn diameters, feed-horn positions, and mirror curvatures. Approximating the mirrors by a thin lens formula and utilizing Gaussian-mode analysis to iterate the various design parameters, a design was achieved that met the initial design constraint of identical patterns at the subreflector.

The resulting design is shown in Fig. 8-2. The feed-horn designs and mirror curvatures are well documented in [6]. A picture of the three operational antennas at Goldstone is shown in Fig. 8-3.

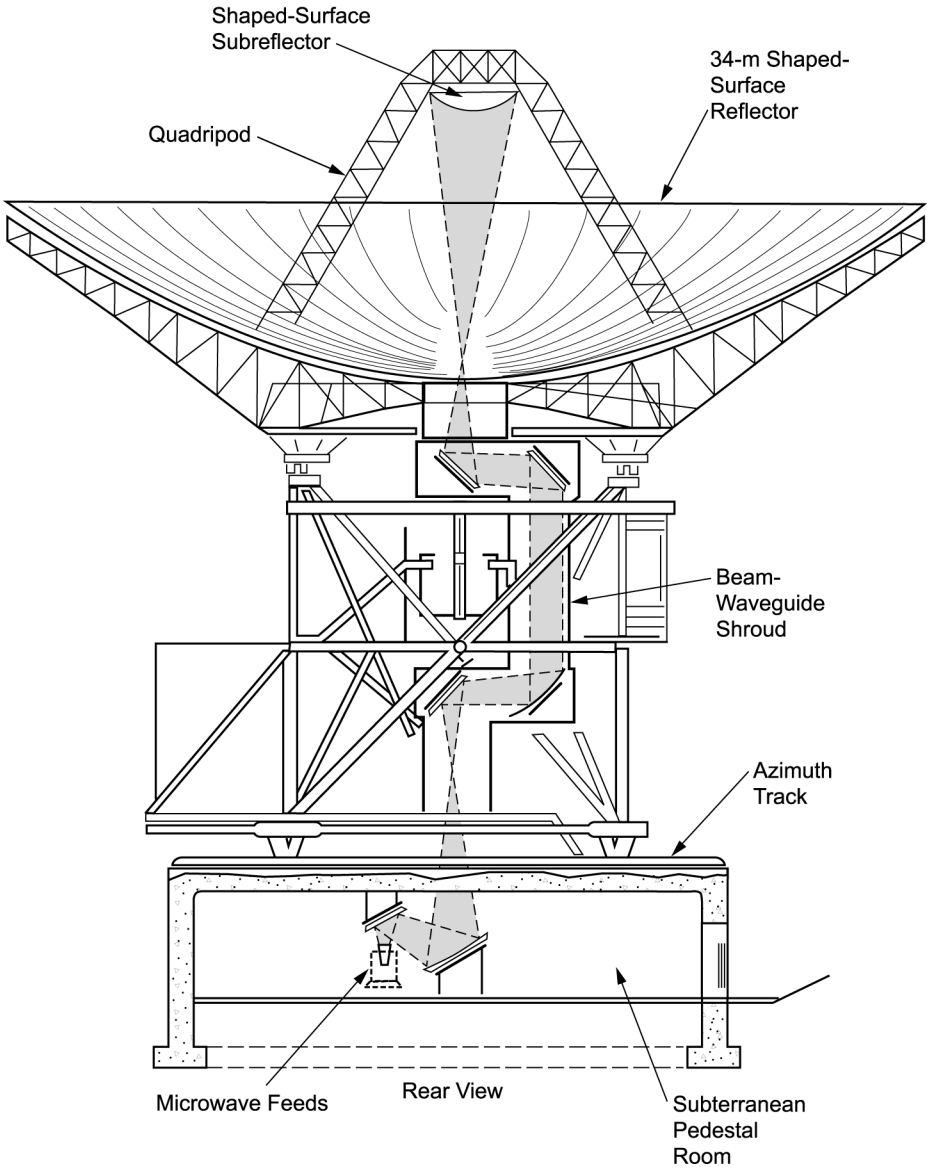

Fig. 8-1. DSS-24 antenna.

8.2 Initial Testing

The radio frequency (RF) performance measurements taken during the start-up of DSS-24 after completion of the antenna construction contract with TIW (now Tripoint Global Communications) is described. The measurements

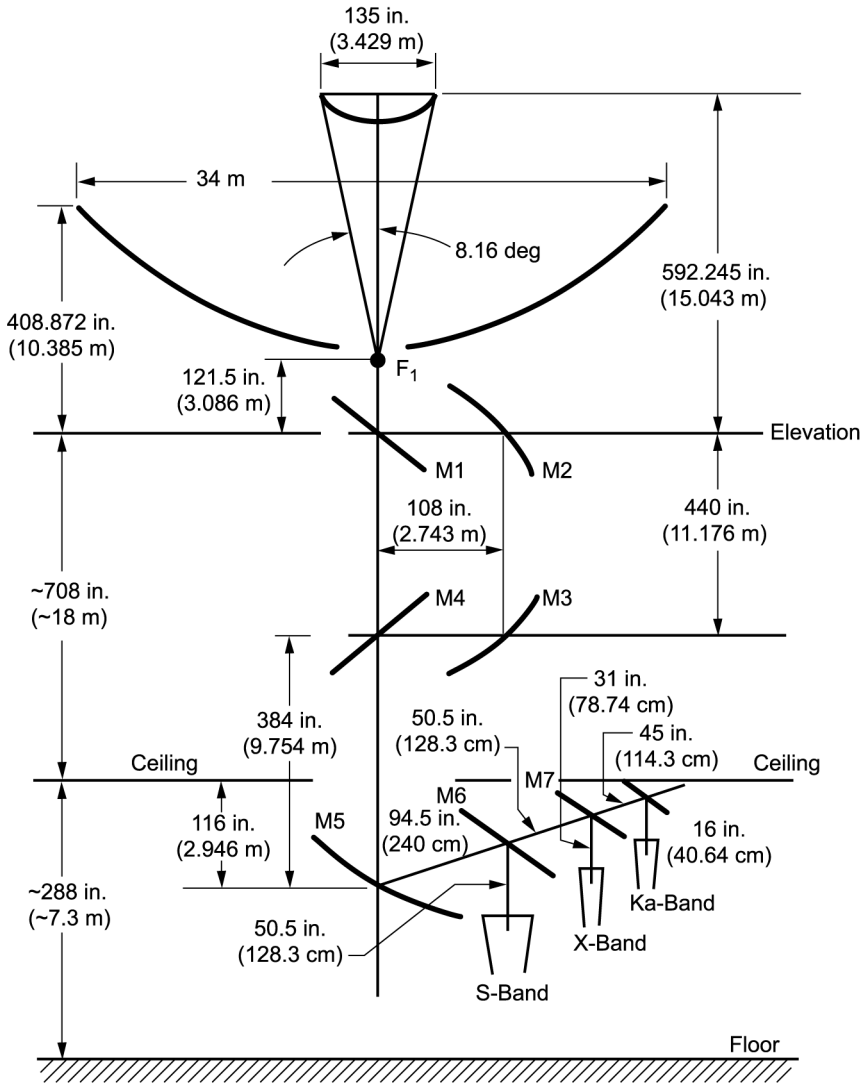

Fig. 8-2. Detailed dimensions of the BWG configuration for DSS-24.

were taken during an intensive 8-week program from May 6 to July 11, 1994, according to a test plan described in [7]. During this period, the antenna mechanical subsystem, the microwave subsystem, and portions of the frequency and timing subsystem were tested as a complete system.

The measurements included microwave holography to verify the surface accuracy of the main reflector and to optimize the position of the subreflector. Aperture efficiency, noise temperature, and pointing accuracy at Ka- and X-bands were measured using the portable test package technique in both the

Fig. 8-3. The three operational BWG antennas at Goldstone, California.

Cassegrain (F_1) configuration and in the normal BWG (F_3) configuration to accurately determine the difference in performance between the two configurations. Additional noise-temperature measurements were taken with the test packages on the ground to measure the actual noise-temperature contribution of the antenna.

X-band and S-band aperture efficiency, noise temperature, and pointing accuracy measurements were also made with the operational feeds installed in the pedestal. The operational feeds were tested in the low-noise, listen-only mode and the S-/X-band mode. During the testing, a systematic error correction model for the antenna-pointing computer (APC) was developed.

The details of the testing are well documented in [8]; therefore, only a brief summary will follow.

8.2.1 Microwave Holography Measurements

The first operational 34-m BWG was named DSS-24 and constructed at Goldstone, California. As part of the construction contract, the antenna panels were approximately set using theodolite measurements, and the subreflector position settings were analytically determined using a theoretical mechanical model. Then the Jet Propulsion Laboratory (JPL) Microwave Antenna Holography System (MAHST) [9] was utilized to provide accurate panel-setting and subreflector position information. Table 8-1 shows the performance improvement achieved by using the data obtained from the MAHST system to reset the panels and update the subreflector position tables. Using MAHST enabled set-

Table 8-1. Performance improvement by microwave holography at 45-deg elevation.

Frequency	Panel Setting (dB)	Subreflector (dB)	Total (dB)
8.45 GHz (X-band)	0.10	0.25	0.35
32 GHz (Ka-band)	1.27	3.60	4.87

ting the main reflector panels of DSS-24 to 0.25 mm root-mean-square (rms), making DSS-24 the highest-precision antenna in the National Aeronautics and Space Administration (NASA)/JPL DSN. The precision of the DSS-24 antenna (diameter/rms) is 1.36×10^5, and the gain limit is 95 GHz.

8.2.2 Efficiency Measurements

In a similar manner to that used for DSS-13, efficiency measurements were made at the F_1 and F_3 focal points, using the R&D test packages at X-band (8.45 GHz) [10] and Ka-band (32 GHz) [11].

Figure 8-4 shows the X-band efficiencies at the F_1 and F_3 focal points as a function of elevation angle. The peak X-band efficiency at F_1 was determined to be 75.25 percent at an elevation angle of 42.5 deg, with a one standard deviation uncertainty of 2.04 percent. The peak X-band efficiency at F_3 was calculated to be 72.67 percent at an elevation angle of 49 deg with a computed uncertainty on the peak efficiency of 1.81 percent.

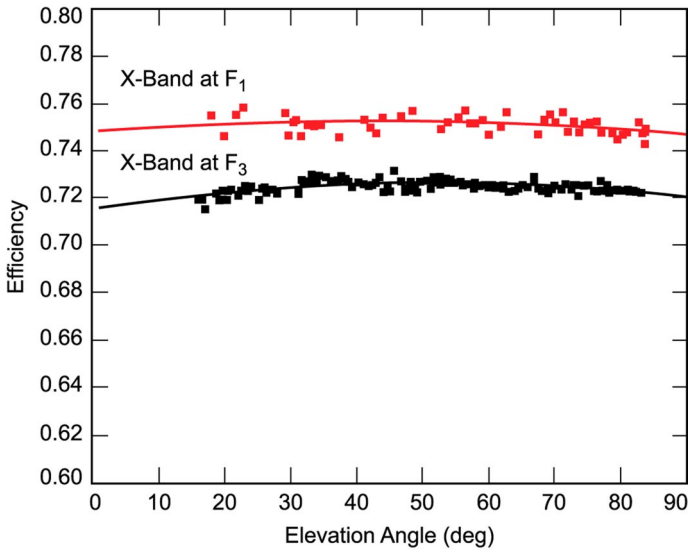

Fig. 8-4. X-band (8.45-GHz) efficiencies at F_1 and F_3 focal points, without atmosphere.

Figure 8-5 shows the Ka-band efficiency measured at F_1 and Fig. 8-6 the efficiency measured at F_3. The Ka-band peak efficiency at F_1 was calculated to be 60.60 percent at an elevation angle of 44.5 deg, with an uncertainty of 2.18 percent. The Ka-band peak efficiency at F_3 was determined to be 57.02 percent at an elevation angle of 42.0 deg, with an uncertainty of 2.51 percent. The gravity-induced roll-off of the F_3 efficiency curve shown in Fig. 8-6 is slightly flatter than that measured at F_1, shown in Fig. 8-5. This is expected since the final subreflector offset curves determined at F_3 with the automated subreflector optimization scheme provided better focusing than those used at F_1. The F_3 gravity loss profile, computed from the best-fit efficiency curve, is shown in Fig. 8-7. It is assumed that there is zero loss at the peak gain elevation angle of 42 deg. Observe that this is significantly better than that of DSS-13 (also shown on Fig. 8-7) and indicates that the redesign of the structure to provide a better match to the finite-element method (FEM) model was successful.

Efficiency measurements were made of the X-band operational feed with the S-/X-band dichroic plate in place. See Fig. 8-8 for a picture of the S-/X-band system and Fig. 8-9 for the efficiency measurements as a function of elevation angle. The peak efficiency was computed to be 71.10 percent, with an estimated uncertainty of 2.31 percent.

S-band efficiency measurements were also made on the operational feed system. Figure 8-10 shows the measurements as a function of elevation angle. The azimuth angles for the data points range from 60 to 295 deg, with southern (180-deg azimuth) transit elevation angles of 67.5 deg for star 3C274 and

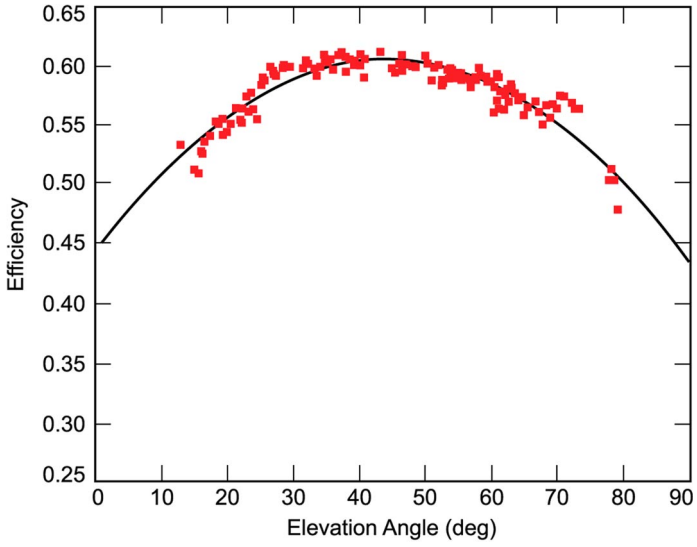

Fig. 8-5. Ka-band (32-GHz) efficiency at F_1 focal point, without atmosphere.

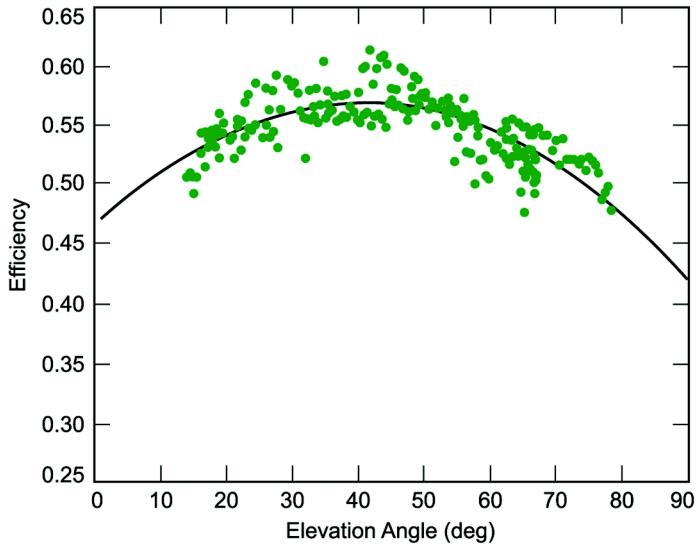

Fig. 8-6. Ka-band (32-GHz) efficiency at F_3 focal point, without atmosphere.

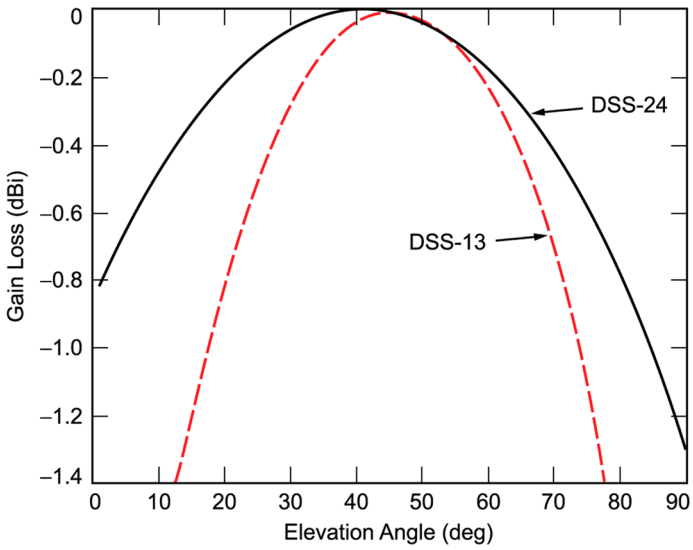

Fig. 8-7. Ka-band gravity loss for the F_3 focal point.

83 deg for star 3C123. The peak S-band efficiency was computed to be 71.50 percent, measured for both sources at the 180-deg azimuth angle. The uncertainty on the peak value is 1.82 percent, which corresponds to a peak S-band gain of 56.79 dBi ± 0.11 dB.

Fig. 8-8. The S-/X-band feed system at DSS-24.

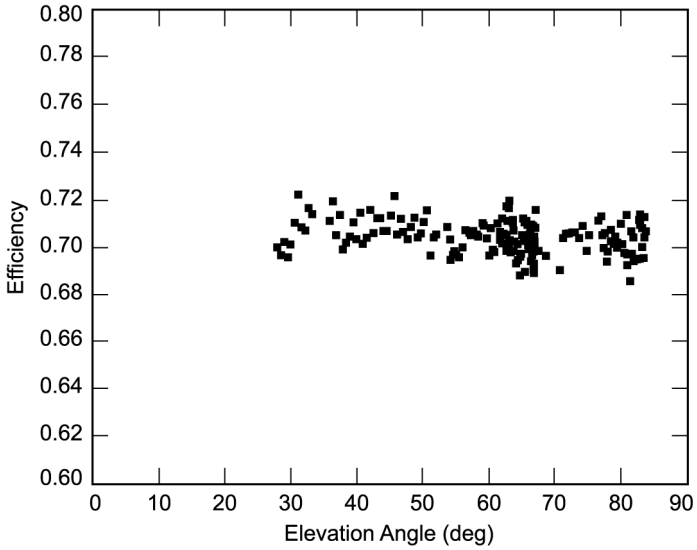

Fig. 8-9. X-band (8.45 GHz) efficiency measurements on the operational feed horn at F_3 focal point, without atmosphere.

The variation of antenna efficiency as a function of azimuth angle is also contained in Fig. 8-10. The peak operational gain at the 180-deg azimuth, was predicted by a previous RF analysis [12] for the S-band feed at the 270-deg pedestal room position. The predicted antenna efficiency variation between the azimuth range of 60 to 295 deg, computed for a perfectly aligned BWG mirror

system, was 2 percent. As measured at DSS-24 and shown in Fig. 8-10, the variation is 4 percent over the same angle range.

The efficiency data is summarized in Table 8-2 for both the R&D and operational feed packages.

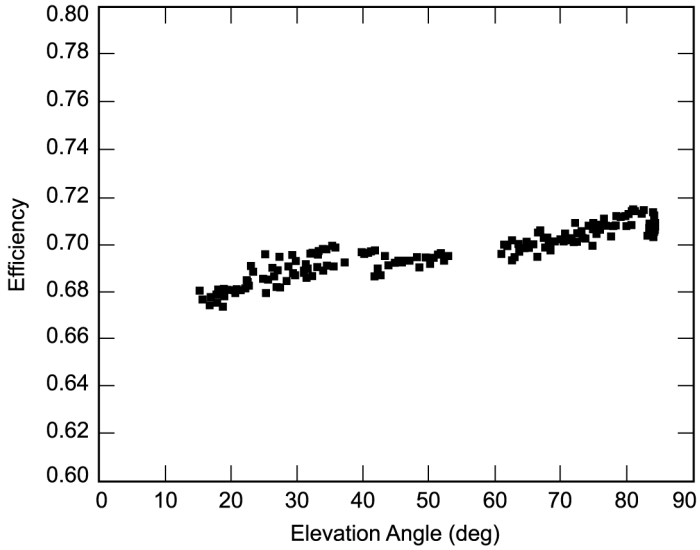

Fig. 8-10. S-band (2.295-GHz) efficiency measurements on the operational feed horn at F_3 focal point, without atmosphere.

Table 8-2. Summary of antenna peak gains and efficiencies at the S-, X-, and Ka-band frequencies.

Frequency and Focal Point	Gain (dBi)	1-Sigma Gain Error (dB)	Efficiency (percent)	1-Sigma Efficiency Error (percent)
8.45 GHz at F_1	68.33	0.12	75.25	2.04
8.45 GHz at F_3	68.19	0.11	72.67	1.81
32 GHz at F_1	78.97	0.16	60.60	2.18
32 GHz at F_3	78.70	0.20	57.02	2.51
8.45 GHz OPS[a] feed at F_3	68.09	0.14	71.10	2.31
2.295 GHz OPS feed at F_3	56.79[b]	0.11	71.50	1.82

[a]Operational.
[b]Measured when at azimuth angle = 180 deg.

8.2.3 Noise-Temperature Results

Noise-temperature measurements were also made with both the R&D test packages and the operational S-/X-band feed system. Table 8-3 shows the measured system-noise-temperature data of these test packages off and on the DSS-24 antenna. If measurements were to be made with the mirrors taped (aluminum tape covering the gap between the central alignment plug and the mirror), the values would be 1–2 K lower than those shown in Table 8-3. Table 8-4 shows the differential noise contribution of the DSS-24 antenna with the data from the DSS-13 antenna for comparison. These values are derived by taking the difference of the system noise temperatures with the test package on the ground, at F_1 and F_3.

Table 8-5 shows the measured noise-temperature data of the operational S-/X-band feed systems in different polarization and feed configurations (that is, diplexed or listen-only, S/X or X only). The operational S-/X-band feed systems cannot be tested at F_1, but differential values for the F_3–ground case are

Table 8-3. Antenna noise-temperature data (K) with R&D test packages. Measurements were made before the taping of M5 and M6. (X-band LNA input temperature = 12 K; Ka-band LNA input temperature = approximately 60 K; Ka-band waveguide feed components temperature contribution = approximately 18 K.)

R&D Feed	F_1	F_3	Ground
X-band	26.6	30.6	21.3
Ka-band	93.1	101.3	86.8

Table 8-4. Antenna noise-temperature contributions: (a) R&D X-band; estimated uncertainty = ± 0.2 K (actual F_3-related values are expected to be 1.4 K lower than shown in the table) and (b) R&D Ka-band; estimated uncertainty = ± 1 K. Measurements for both were made before mirror taping of M5 and M6.

Antenna	(a) R&D X-band Temperature (K)		
	F_1 – Ground	$F_3 – F_1$	F_3 – Ground
DSS-24	5.3	4	9.3
DSS-13	3.2	2.4	5.6
	(b) R&D Ka-band Temperature (K)		
	F_1 – Ground	$F_3 – F_1$	F_3 – Ground
DSS-24	6.3	8.2	14.5
DSS-13	7.1	6.8	13.9

Table 8-5. Noise temperature data using operational feed horns: (a) S-band (2.295 GHz) antenna and (b) X-band (8.420 GHz) antenna.

(a) S-Band[a]

Polarization	Configuration	F_3 Noise Temperature (K)	F_3 – Ground (K)
RCP	Low-noise	30.8	15
LCP	Low-noise	30.6	Not measured
RCP	Diplexed	37.3	15
LCP	Diplexed	37.0	Not measured

[a] S-band LNA temperature = 5.5 K; follow-on temperature = 0.2 K.
S-band measurements performed before mirror taping of M5 and M6; actual noise temperature is expected to be 0–1 K lower than above.
Estimated uncertainty = ± 1 K.

(b) X-Band[b]

Polarization	Configuration	F_3 Noise Temperature (K)	F_3 – Ground (K)
RCP	Low-noise	25.5	10
LCP	Low-noise	25.2	Not measured
RCP	S-/X-band	27.0	12
LCP	S-/X-band	26.5	Not measured

[b] X-band LNA temperature = 3.2 K; follow-on temperature = 0.1 K.
Above values include mirror taping of M5 and M6, noise reduction of 1.4 K.
Estimated uncertainty = ± 1 K.
F_3 – ground values derived from testing performed with feed horn at JPL.

included. The ground measurements were made at JPL as part of the feed acceptance testing [13]. These measurements were corrected for the atmospheric difference between DSS-24 and JPL. A noise budget for the X-band operational feed horn is shown in Table 8-6. System-noise temperature of the operational S-/X- and Ka-band feed systems as a function of elevation angle is shown in Fig. 8-11 (all other noise measurements were made at zenith elevation angle).

8.2.4 The Shroud

One of the requirements for versatility on the BWG antenna was to be able to upgrade or repair electronics not currently in use in the pedestal room while the antenna was otherwise transmitting. This could be the case if there was a second feed system in the BWG similar to the multiple feed systems in the DSS-13 BWG. This might be accomplished if the beam path was enclosed in a

Table 8-6. Antenna system-noise-temperature frequency budget using X-band operational feed. T_{maser} = 3.5 K and $T_{follow\text{-}on}$ = 0.1 K.

Source	Contribution (K)	Difference from 890-261 [14] Predicted (K)
Cosmic background	2.5	0.0
Atmosphere	2.5	0.0
Main and subreflectors	5.3	1.4 (3.9)
BWG	4.0	1.6 (2.4)
S-/X-band dichroic plate	1.5	–1.8 (3.3)
Mirror tape	–1.5	–1.5
Feed/LNA	12.4	0.0
Total	26.7	–0.3

metal shield so that energy scattered off the edge of the BWG mirrors could be contained.

The selected design was a metal shroud enclosure in the form of an inverted pyramid; it was installed around the basement ellipse, as shown in Fig. 8-12. The apertures of the feed horn penetrate the shroud, and the radiated beam is entirely enclosed and separated from the rest of the pedestal room. A survey was made on the radiated power in the pedestal room outside the shroud, and it was determined that the levels were below the accepted 1 mW/cm^2 standard for

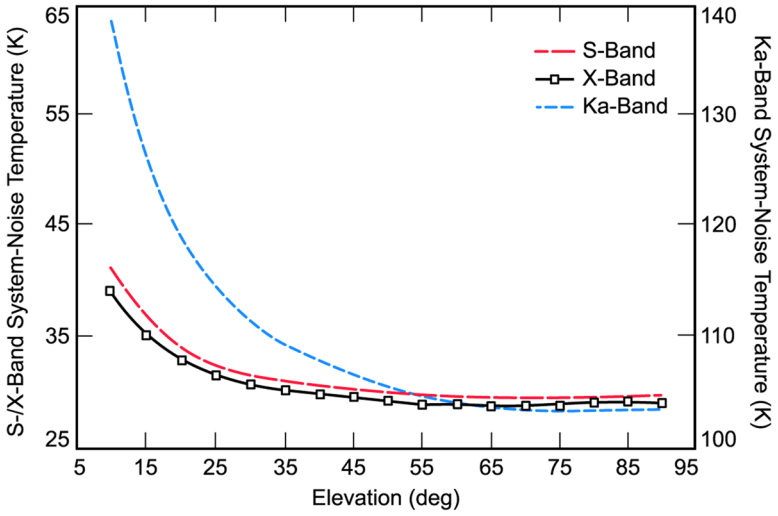

Fig. 8-11. System-noise temperature as a function of elevation angle.

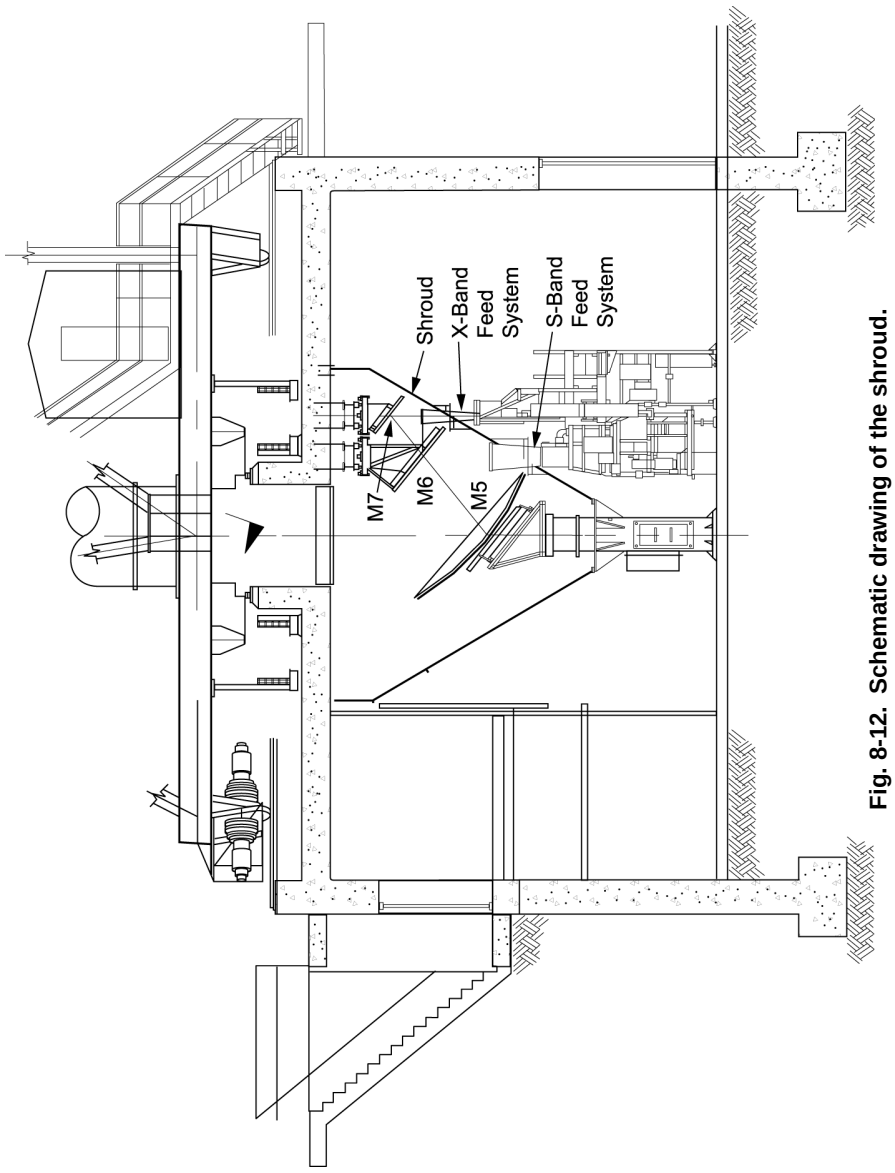

Fig. 8-12. Schematic drawing of the shroud.

safety. Hence, it is quite safe to be in the pedestal room when the antenna is transmitting. A photograph of the DSS-24 shroud is shown in Fig. 8-13.

8.3 Adding Ka-Band to the Operational 34-Meter Beam-Waveguide Antennas

There are two different implementations of Ka-band in the operational network: a Ka-band system installed at DSS-25 at Goldstone, California, in support of Cassini Project radio science and a second, yet-to-be-installed (as of 2002) system intended for all the other BWG systems. The Ka-band system at DSS-25 includes Ka-band transmit-and-receive capability and utilizes separate Ka-band feed horns for transmit-and-receive, with a dichroic plate to separate the frequencies. The system intended for the rest of the network is receive-only at Ka-band and includes a multifrequency X-/X-/Ka-band feed that also provides a feed diplexing system for X-band. In 1999, an engineering model of the front end was constructed and tested at DSS-26 (also at Goldstone, California); it validated the design.

8.3.1 The Cassini Radio Science Ka-Band Ground System

A schematic of the basic geometry for the X-/Ka-band system at DSS-25 is shown in Fig. 8-14. Additions to the BWG baseline design include transmit-and-receive Ka-band feed horns, a Ka-/Ka-band dichroic plate (M8), an X-/Ka-band dichroic plate (M7), and a hyperboloidal mirror (M9) [15].

Fig. 8-13. The shroud at DSS-24.

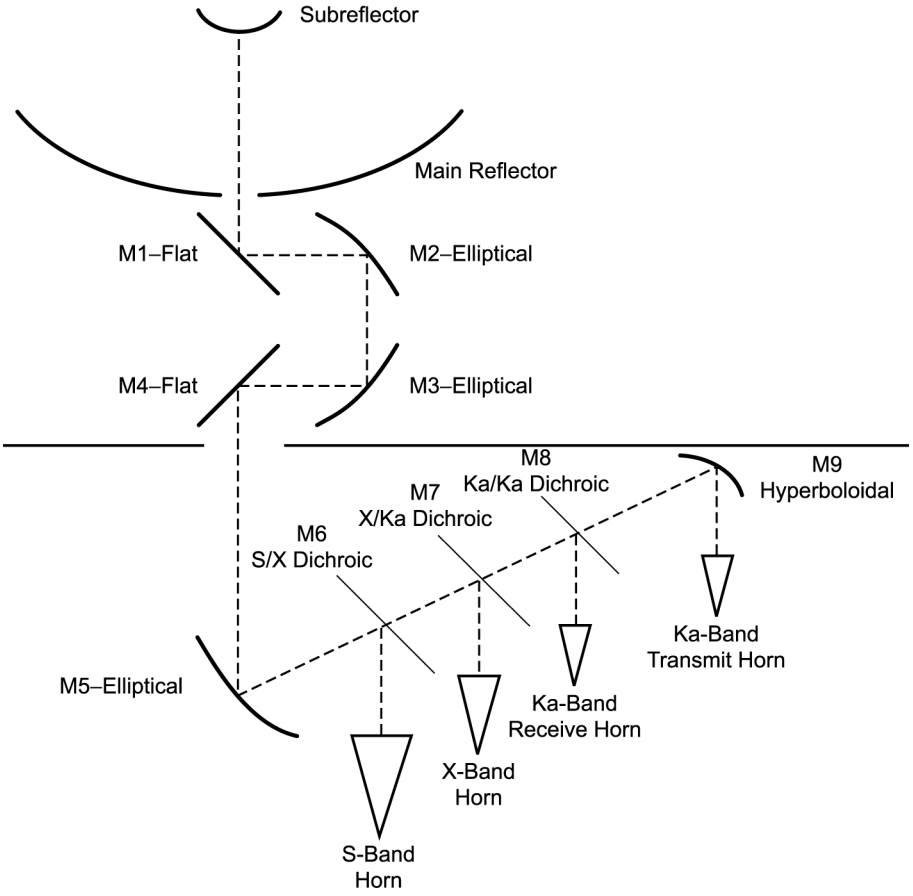

Fig. 8-14. Basic geometry of DSS-25.

8.3.1.1 Optics Design. For an initial sizing of the Ka-band receive horn, the focal-plane-analysis method was used [1]. The Cassegrain shaping pattern was used to excite the BWG from F_1 in a receive-mode analysis. The far-zone horn pattern that maximizes the antenna gain is the far-zone pattern produced by the complex conjugate of the PO currents on M5 (or the focal plane at F_3). A horn gain of 30.3 dBi produces the maximum gain; however, the significant antenna performance parameter is G/T_{sys}. The antenna performance (G/T_{sys}) was calculated for several gain feed horns (Table 8-7) around the maximum gain horn, and a horn design with 31.47-dB gain was chosen because it yielded the maximum G/T_{sys} and is for all practical purposes a maximum-gain horn.

The DSS-25 basement ceiling is very close to the M5 focus, and using an M9 flat mirror does not allow enough space for the transmit horn, as approxi-

Table 8-7. Dependence of DSS-25 Ka-band receive performance on feed-horn gain.

Horn Gain (dBi)	BWG Spill (percent)	Subreflector Spill (percent)	Main Reflector Spill[a] (percent)	Noise Temperature (K)	Gain (dBi)	$\Delta(G/T_{sys})$[b] (dB)
29.3	1.07	3.29	1.60	6.81	80.64	–0.11
30.46	0.77	2.80	1.45	5.66	80.62	+0.00
30.96	0.52	2.09	1.04	3.98	80.67	+0.16
31.47	0.34	1.57	0.94	3.25	80.63	+0.23
31.47[c]	0.24	1.18	0.68	2.34	80.72	+0.32

[a] Main reflector spillover values were computed using an insufficient number of integration steps.
[b] $\Delta(G/T_{sys})$ values were computed using S. Slobin's parameters as described by Veruttipong in [14] for LNA temperature, ohmic losses, atmospheric attenuation, etc.
[c] Feed refocused.

mately 38 cm is needed between the receive and transmit horn axes to accommodate the corresponding amplifiers. Also, the size of the X-band feed horn and its amplifier does not allow the Ka-band receive horn to be moved closer to M5 to create more space for the Ka-band transmit horn. A solution to the lack-of-space difficulty, without sacrificing antenna performance, is to use a lower-gain horn for transmit in conjunction with a gain-magnifying mirror for M9 (i.e., a concave hyperboloidal mirror). A lower-gain horn is physically smaller and has a phase center closer to its aperture, allowing more clearance between the horn aperture and M9. An M9 mirror that magnified the horn gain by approximately 3.5 dB was selected to accommodate the required horn and amplifiers. This yielded a horn gain of approximately 26.9 dB. The overall antenna gain was calculated with a variety of horn gains, and it was determined that the overall antenna gain is only weakly dependent on the horn gain. A horn of 26.64 dBi was selected for the design.

The M7 dichroic mirror utilizes the same design as that used for DSS-13. To reduce manufacturing costs, a 30-dB rim taper was adopted for the perforated regions of all dichroic mirrors. The Ka-band transmit mode determines the dimensions of the M7 perforated region and yields an elliptical area approximately 94.5 by 81.8 cm.

The M8 dichroic plate was designed to pass Ka-band uplink (34.2–34.7 GHz) and to reflect the downlink (31.8–32.3 GHz). The plate utilized stepped apertures [16] in order to separate the two-frequency band with only a 1:1.07 ratio. The geometry of the five-layer plate is shown in Fig. 8-15; the measured and calculated reflection coefficient versus frequency for circular polarization is shown in Fig. 8-16.

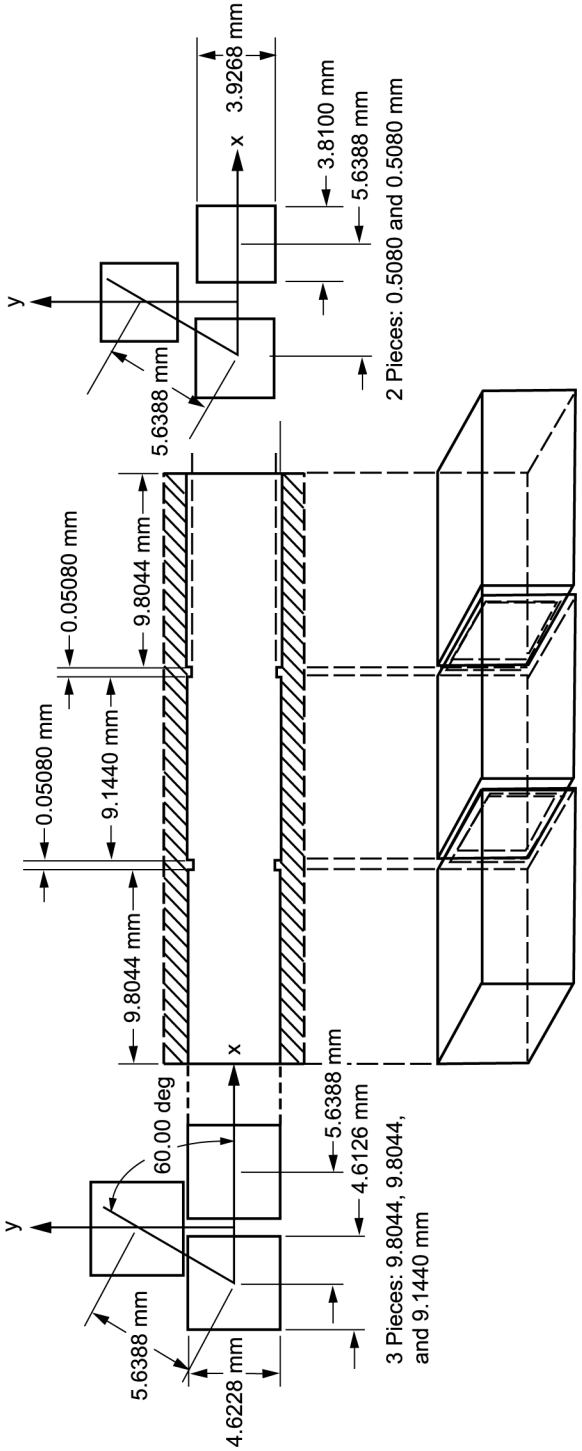

Fig. 8-15. Layout of the holes and hole pattern for the five-layer Ka-band dichroic plate.

8.3.1.2 Monopulse Pointing System. Traditionally, the DSN has employed the conical scanning (CONSCAN) algorithm for pointing the antennas at 2.2–2.305 GHz (S-band) and 8.2–8.6 GHz (X-band). In CONSCAN, the pointing error is estimated by moving the antenna in a circle with respect to the best estimate of the spacecraft location. The received power detected on this circle is used to generate a new best estimate of the spacecraft location. Nominally, the circle chosen is such that the detected power is 0.1 dB less than the peak of the antenna beam. In the BWG antennas, the 0.1-dB beamwidths are 22 mdeg at S-band (2.295 GHz), 5.9 mdeg at X-band (8.45 GHz), and 1.5 mdeg at Ka-band (32 GHz). At S- and X-band frequencies, a typical jitter of 1 mdeg in the antenna pointing (under favorable environmental conditions, with no wind) does not result in significant fluctuations in detected power levels. At Ka-band, the same jitter causes significant fluctuations in the detected power levels; these fluctuations are not acceptable for radio science application. For this reason, it became necessary to adopt a new technique that allowed the antenna to be pointed directly at the spacecraft. An additional advantage is a 0.1-dB gain in signal by not having to point away from the spacecraft.

The selected pointing system uses a single feed horn and a monopulse tracking coupler, as shown in Fig. 8-17. This coupler has both a sum port (TE_{11} mode) and a difference port (TE_{21} mode). As described in [17], the TE_{21} mode is excited by means of eight symmetrically placed Ka-band waveguides, which are, in turn, connected through a series of combiners to generate circular polarization. When radiated by the corrugated horn, the TE_{21} mode has a theoretical

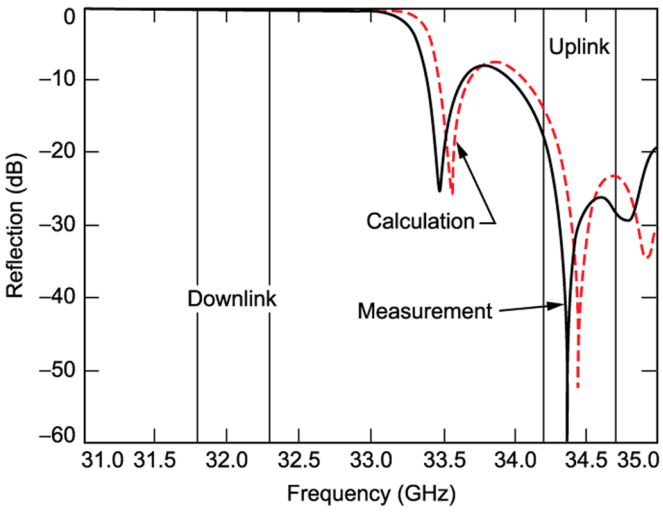

Fig. 8-16. Performance of the five-layer Ka-band dichroic plate.

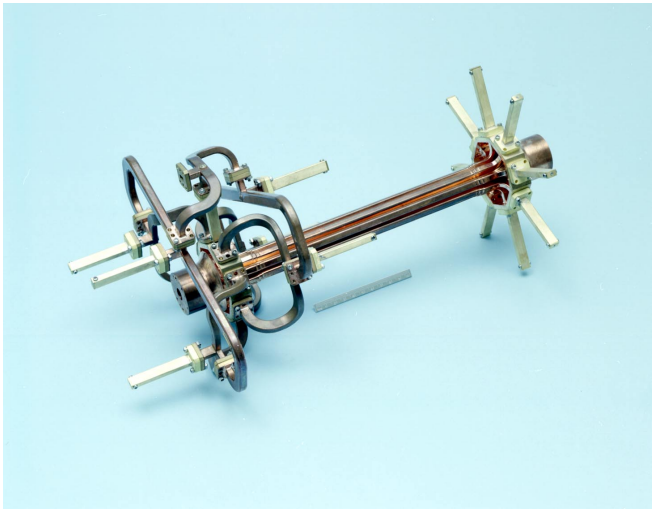

Fig. 8-17. Ka-band monopulse coupler.

null on axis. The magnitude of the power received in the TE_{21} mode relative to the TE_{11} mode (sum beam) is proportional to the θ pointing error (angle relative to the antenna boresite—see Fig. 8-18). The azimuthal error, ϕ, is proportional to the phase difference between the sum and difference signals. Thus, by measuring the complex ratio of the sum and difference signals, pointing updates can be generated that will drive the difference signal and, consequently, the antenna pointing error to zero.

An additional consideration in a BWG antenna is that there is a rotation of the coordinate system from the feed system to the reflector system. The tracking coupler measures the ϕ angle in the feed coordinate system. The ϕ angle in the reflector system rotates linearly with both the azimuth and elevation motion of the antenna.

The performance of the monopulse pointing system of the 34-m BWG antennas is well documented in [18].

8.3.1.3 Measured Performance After Installation of Ka-Band. The measured efficiencies before installation of Ka-band (single-frequency system) were R&D X-band 76.6 percent, operational X-band 76.5 percent, and R&D Ka-band 57.5 percent [19].

After M7 dichroic installation (X-/Ka-band feed system), the measured efficiencies were 75.5 percent for X-band and 57.9 percent for Ka-band.

The noise temperature of the maser amplifier system at X-band was measured with M7 as a flat plate, 23.8 K; and with M7 as the X-/Ka-band dichroic plate, 23.6 K.

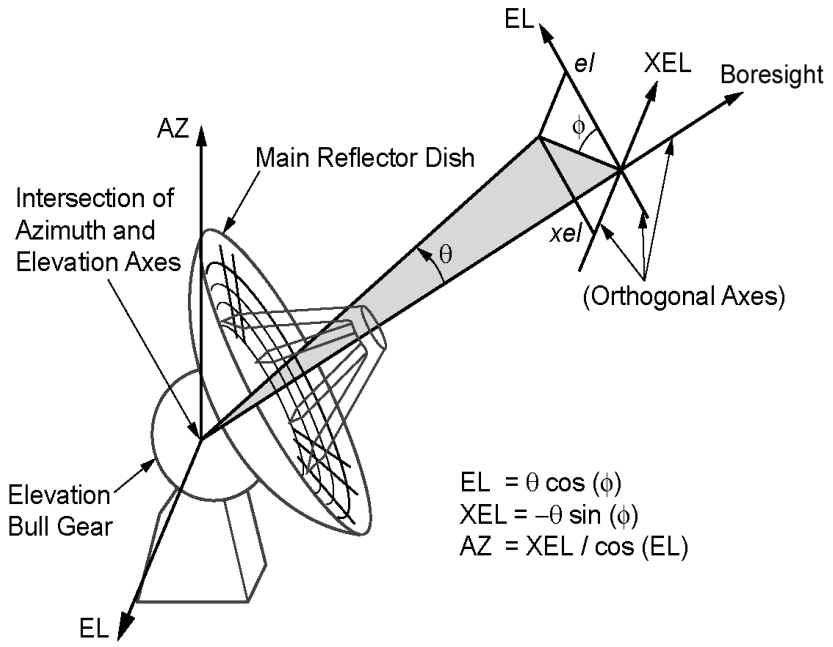

Fig. 8-18. The relationship between the multiple coordinate systems within the monopulse implementation.

The system-noise temperature of the Ka-band feed horn at DSS-25 was measured with the indium phosphide high-electron-mobility-transistor (HEMT) technology low-noise-amplifier (LNA) module [20]. The LNA module has an input noise temperature of 12.3 K and represents the debut of this technology in the DSN.

Measurement of the LNA package input noise temperature, T_e (referenced at the feed-horn aperture), was accomplished using a Y factor method. An ambient load and a liquid-nitrogen-cooled load were used as reference power sources. A 32-GHz measurement made at JPL was 20.2 K; when repeated at DSS-25, it was 19.9 K.

Measurements were also made of the total system-noise temperature (T_{op}), both outside the antenna and in its final installed position inside the antenna. The average T_{op} measured outside the antenna was 34.6 K at 32 GHz. Subtracting the measured T_e of 20 K results in a sky-noise temperature of 14.6 K. The measured T_{op} with the feed horn installed in its final operational position was 45.0 K. Using the measured air temperature and humidity, the sky-noise temperature was estimated to be 11.7 K. The sky noise measured by the water vapor radiometer at DSS-13 at 31 GHz was 10 K. Subtracting the measured T_e of 20 K and the estimated sky-noise temperature of 10–12 K results in an antenna noise temperature of 13 to 15 K.

8.3.1.4 Beam-Aberration Correction. The aberration effect occurs when the uplink and downlink beams must be pointed in different directions for simultaneous uplink and downlink communications. It arises solely from the fact that a spacecraft is moving in the right-ascension/declination (RA/DEC) coordinate system as seen from a point (the antenna) on Earth. At any instant of time, the downlink beam must be pointed where the spacecraft was one round-trip light time (RTLT) ago, and the uplink beam must be pointed where the spacecraft will be in one RTLT. Kurt Liewer [21] was the first person to draw attention to the fact that aberration effects on the radio link between a ground station and a spacecraft must result in an offset angle between the optimal uplink and downlink directions. For Saturn and Earth, this results in a distinct aberration effect (the angular distance between the two RA/DEC positions), with a period of about 400 days. The maximum aberration effect due to planetary motion of the Earth/Saturn is about 15 mdeg. At S- and X-bands, the loss due to this separation of pointing directions is small because the beamwidths of the 34-m antenna are approximately 230 mdeg at S-band and 64 mdeg at X-band. At Ka-band, however, the loss can be as large as 10 dB for a 15-mdeg offset.

In order to obtain uplink and downlink communications in the presence of planetary aberration, it is required that the receive beam be pointed at the predicted spacecraft position (position 1 on Fig. 8-19) and the transmit beam be pointed at the spacecraft position according to the space aberration correction

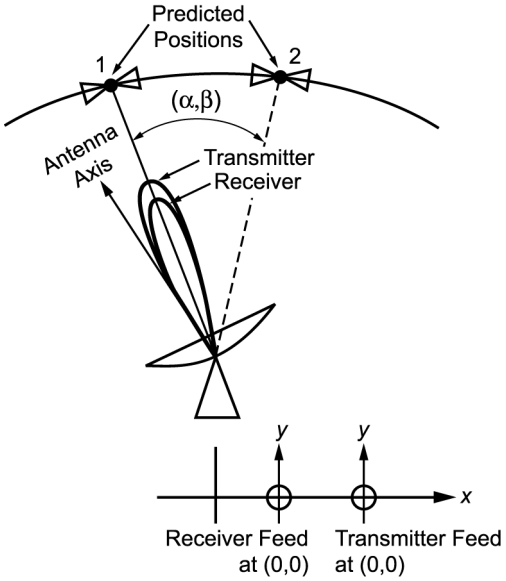

Fig. 8-19. Without antenna-pointing correction for beam aberration.

(position 2). With no correction, both feed horns will be at their nominal positions, termed (0,0). The separation of the feed horns in space is due to the dichroic mirror that separates the transmit and receive frequencies. The relative position between the receive and transmit beams required for aberration correction is identical to the relative position between the two spacecraft positions, which is defined by (α,β) regardless of how we point the antenna. Repointing of one beam with respect to the other can be accomplished by either tilting the mirrors above the feed horn or moving the feeds. For minimum effect on the downlink performance, the option selected was to move the transmit feed horn and klystron. Thus, with correction, the transmit feed is moved a distance (x,y), depending on the predicted correction (α,β), as shown in Fig. 8-20. The required angles for the Cassini mission are given in [22].

Due to the complex relationship between the (x,y) position of the feed horn and the beam pointing direction, a conceptual demonstration of the beam aberration and point-ahead capability was performed at DSS-13. The demonstration was first done at X-band in the receive mode. The antenna was pointed at an X-band source, then moved off source by a known (α,β). The position of the source was recovered by the (x,y) motion of the feed system calculated from the aberration correction model. The experiment was repeated at Ka-band, with the beam maintained on source to within the accuracy of the blind pointing model.

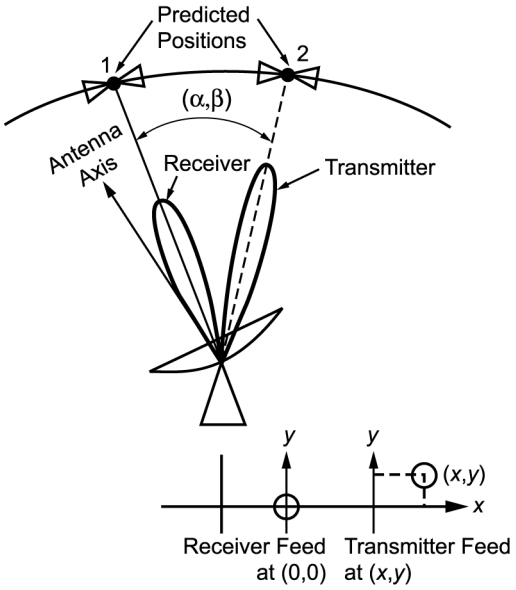

Fig. 8-20. With antenna-pointing correction (by moving the feed horn) for beam aberration.

In DSS-25, the Ka-band feed horn and transmitter were mounted on an "x,y table," and the connection to the shroud was made with a flexible cloth. In June 2001, the system was successfully used with both the Cassini Gravity Wave System tests and the Solar Conjunction System test. It will be used for both the Gravity Wave and Solar Conjunction Experiments.

8.3.2 Ka-Band Upgrades—Receive-Only System

The Cassini radio science system uses a frequency-selective surface (FSS) to separate the X-band and Ka-band signals [23]. This approach has the advantage of requiring relatively simple X- and Ka-band feed horns. Disadvantages include the real estate required for the two feed horns, the need for separate dewars for the X- and Ka-band LNAs, and the noise added due to scattering from the FSS used to diplex the signals.

To overcome these disadvantages, a single feed horn that accommodates all the required frequencies in one package was developed [24]. This feed horn provides for the Ka-band receive signal as well as diplexing the X-band transmit and receive signals. A monopulse tracking coupler is also utilized for Ka-band pointing. This feed system is compact and has low noise relative to separating the X- and Ka-band signals with an FSS. Also, a single, but larger dewar, is used to house all of the LNAs. An additional complication in the design of the feed horn is that the phase center of the feed horn at X-band is not coincident with the phase center at Ka-band, as the positions of the phase centers are prescribed by the BWG geometry.

8.3.2.1 X-/X-/Ka-Band Feed. Figure 8-21 shows a photograph of the X-/X-/Ka-band horn with monopulse coupler and linear polarization combiners attached to the X-band ports. The basic internal configuration of the X-/X-/Ka-band feed horn is shown in Fig. 8-22.

The feed horn is fed at Ka-band through a monopulse coupler, similar in design to that described in [17]. The sum mode at Ka-band, a circularly polarized TE_{11} mode, is excited using a commercial orthomode junction and polarizer. The sum mode passes through the center of the monopulse coupler and enters the horn, as shown at the left in Fig. 8-22. The difference mode, a circularly polarized TE_{21} mode, is excited through the monopulse coupler arms and enters the feed horn as well. These modes are transformed to the hybrid HE_{11} and HE_{21} modes in the Ka-band mode-converter section. The X-band downlink signal is extracted in the X-band downlink junction, which consists of four waveguides that exit the circular guide radially at 90-deg intervals. These waveguides excite a pair of orthogonal TE_{11} modes in the feed horn. A straight corrugated section and slight flare follow. The X-band uplink signal is injected in the X-band uplink junction, which is similar in design to the downlink junction. Next the TE_{11} modes at X-band are transformed into the HE_{11} mode in the

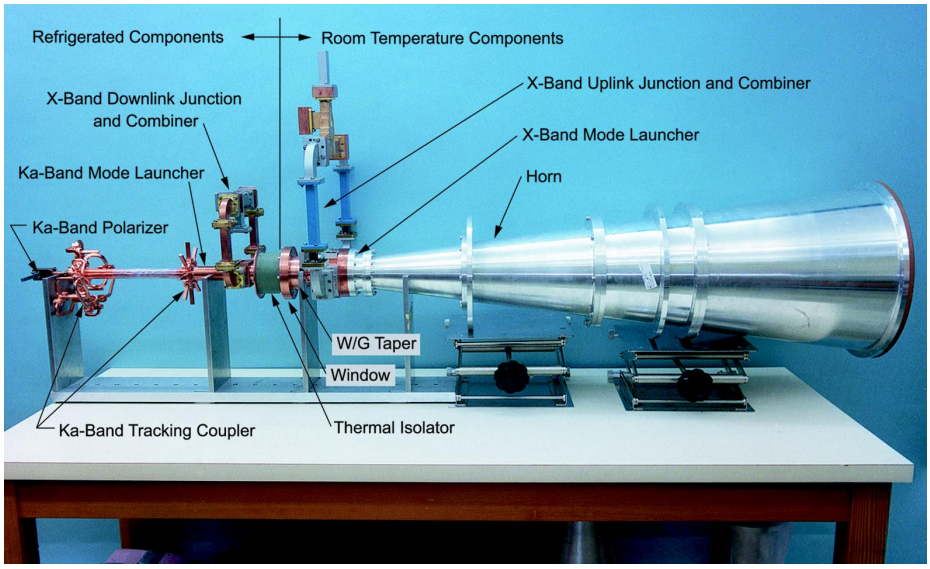

Fig. 8-21. The X-/X-/Ka-band feed horn with monopulse coupler.

X-band mode-converter section. Finally, the feed horn flares at a constant angle with a constant groove profile to the final aperture size. Stanton [24] describes the various feed-horn components in greater detail.

8.3.2.2 BWG Geometry. Only minimal changes in the existing S-/X-band BWG optics is required to incorporate the X-/X-/Ka-band feed horn. This feed horn is just a direct replacement for the existing X-band feed horn. A slight modification of the shroud interface is required to accommodate the different-size feed aperture. The feed system layout is shown in Fig. 8-23.

8.3.2.3 Demonstration at DSS-26. A breadboard X-/X-/Ka-band feed horn was fabricated and tested on DSS-26. The predicted efficiency at X-band was 72.5 percent, and the predicted noise temperature at zenith was 19.83 K. The predicted efficiency at Ka-band is 58.7 percent, with a noise temperature of 37.8 K at zenith [25]. The early tests indicated some problems with the initial feed-horn design, as the noise temperature was 4 K too high at Ka-band and it did not meet the bandwidth requirements at X-band. This led to several redesigns that are discussed in depth in [24]. The design modifications included (a) a new X-band mode launcher design that required only two corrugations instead of seven, (b) the external room temperature waveguides reduced 4.1 in. (10.4 cm) in length, (c) the window and thermal isolator integrated into one component, and (d) the X-band downlink junction modified to a dual-slot design to improve bandwidth and impedance match.

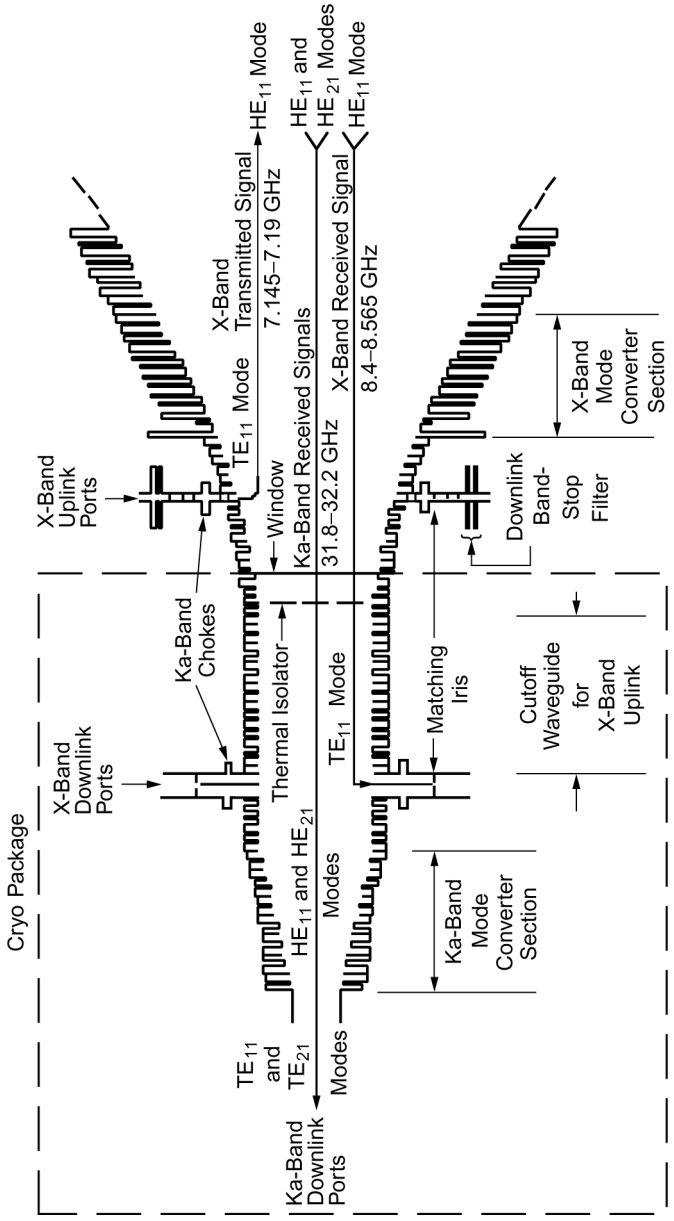

Fig. 8-22. The X-/X-/Ka-band feed horn internal geometry.

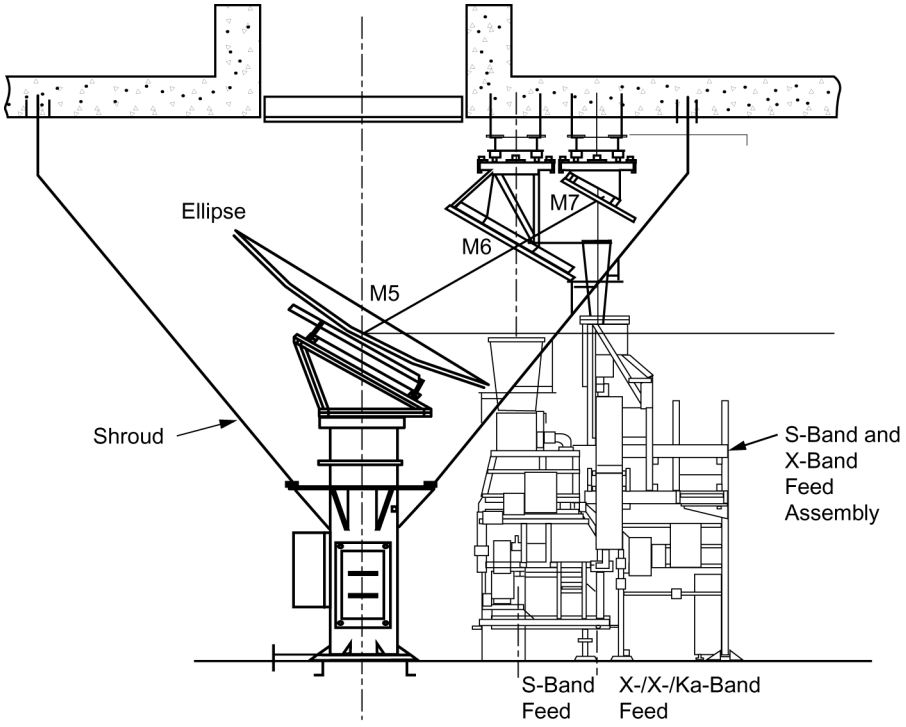

Fig. 8-23. Feed-system layout at DSS-26.

Efficiency measurements were made at DSS-26 with the modified X-/X-/Ka-band feed horn and are shown in Fig. 8-24. A problem was discovered with the subreflector position mechanism and subsequently corrected. After the subreflector fix, the efficiencies (72 percent at X-band and 58 percent at Ka-band) were comparable to those of DSS-25 and the predicted values of 72.5 percent and 58.7 percent, respectively.

Noise-temperature measurements were also made at DSS-26. The data is given in Table 8-8. There was an unaccounted-for antenna noise temperature at X-band. The problem was traced to an untaped center plug on M7. After taping, T_{ant} dropped by 6.6 K at X-band and by 0.9 K at Ka-band. After taping, T_{ant} was 6.4 K at X-band and 10.2 K at Ka-band.

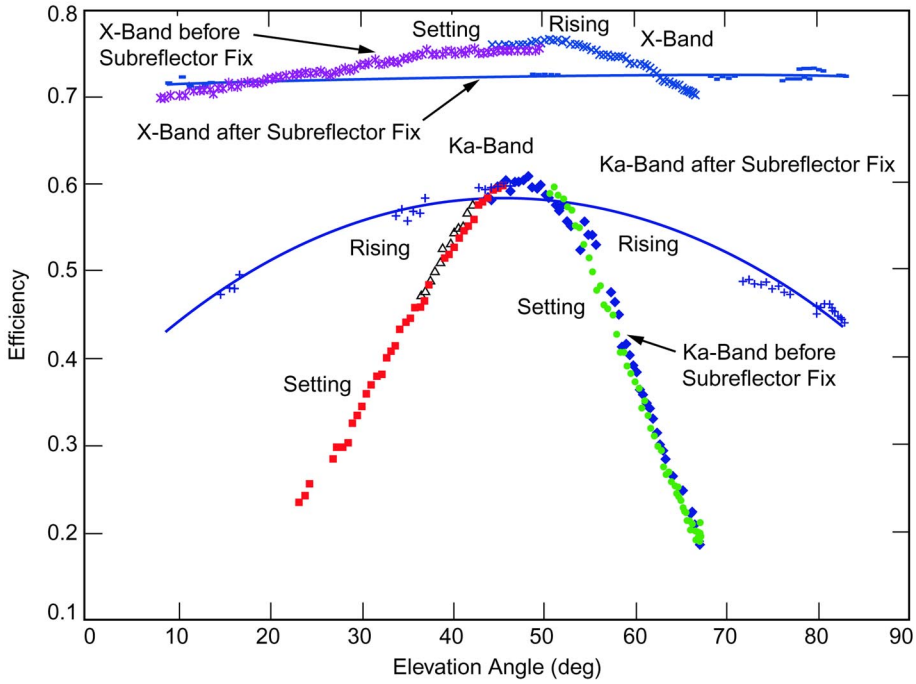

Fig. 8-24. DSS-26 operational X-/X-/Ka-band feed efficiencies.

Table 8-8. Noise-temperature measurements of the X-/X-/Ka-band feed horn at DSS-26. At X-band, 5.8 K was unaccounted for. The problem was traced to an untaped center plug on M7.

Noise Component	Noise Temperature (K)		
	X-Band (8.425 GHz)	Ka-Band (32 GHz)	
	Feed System	Sum Channel	Error Channel
T_e (feed/LNA)	16.4	16.8	25.4
T_{op}	34.3	39.4	47.2
T_{ant} before taping	13.0	11.1	10.2
T_{ant} after taping	6.4	10.2	Not measured

References

[1] W. A. Imbriale, M. S. Esquivel, and F. Manshadi, "Novel Solutions to Low-Frequency Problems with Geometrically Designed Beam-Waveguide Systems," *IEEE Transactions on Antennas and Propagation*, vol. 46, no. 12, pp. 1790–1796, December 1998.

[2] S. R. Rengarajan, V. Galindo-Israel, and W. A. Imbriale, "Amplitude and Phase-Shaping Effects in Beamwaveguides," *IEEE Transactions on Antennas and Propagation*, vol. 39, no. 5, pp. 687–690, May 1991.

[3] W. Imbriale and D. Hoppe, "Computational Techniques for Beam-waveguide Systems," *2000 IEEE Antennas Propagation Society International Symposium*, Salt Lake City, Utah, pp. 1894–1897, July 16–21, 2000.

[4] W. Imbriale and D. Hoppe, "Recent Trends in the Analysis of Quasioptical Systems," *Millennium Conference on Antennas and Propagation*, Davos, Switzerland, April 9–14, 2000.

[5] W. Veruttipong, J. C. Chen, and D. A. Bathker, "Gaussian Beam and Physical Optics Iteration Technique for Wideband Beam Waveguide Feed Design," *Telecommunications and Data Acquisition Progress Report 42-105*, vol. January–March 1991, http://tmo.jpl.nasa.gov/progress_report/issues.html Accessed October 2001.

[6] W. Veruttipong, "RF Design and Expected Performance of a 34-meter Multi-frequency Beam-Waveguide Antenna," JPL D-11853 (internal document), Jet Propulsion Laboratory, Pasadena, California, July 15, 1994.

[7] *DSS-24 RF Performance Test Plan*, DSN document 829-6 (internal document), Jet Propulsion Laboratory, Pasadena, California, January 1994.

[8] M. J. Britcliffe, *DSS-24 Antenna RF Performance Measurements*, JPL D-12277 (internal document), Jet Propulsion Laboratory, Pasadena, California, February 1, 1995.

[9] D. J. Rochblatt, P. M. Withington, and H. J. Jackson, "DSS-24 Microwave Holography Measurements," *Telecommunications and Data Acquisition Progress Report 42-121*, vol. January–March 1995, http://tmo.jpl.nasa.gov/progress_report/issues.html Accessed October 2001.

[10] T. Y. Otoshi, S. R. Stewart, and M. M. Franco, "A Portable X-Band Front-End Test Package for Beam Waveguide Antenna Performance Evaluation, Part I: Design and Ground Tests," *Telecommunications and Data Acquisition Progress Report 42-103*, vol. July–September 1990, http://tmo.jpl.nasa.gov/progress_report/issues.html Accessed October 2001.

[11] T. Y. Otoshi, S. R. Stewart, and M. M. Franco, "A Portable Ka-Band Front-End Test Package for Beam Waveguide Antenna Performance Eval-

uation, Part I: Design and Ground Tests," *Telecommunications and Data Acquisition Progress Report 42-106*, vol. April–June 1991, http://tmo.jpl.nasa.gov/progress_report/issues.html Accessed October 2001.

[12] W. Veruttipong, "S-band Efficiency and G/T Performance for Various Azimuth Positions," JPL Interoffice Memorandum 3327-94-113 (internal document), Jet Propulsion Laboratory, Pasadena, California, June 9, 1994.

[13] M. Gatti, "RF Characterization and Testing of the DSS-24 Feed Group S- and X-band Feeds," JPL Interoffice Memorandum 3320-94-101, Jet Propulsion Laboratory, Pasadena, California, March 2, 1994.

[14] W. Veruttipong, "RF Design and Expected Performances of a 34-Meter Multifrequency Beam-Waveguide Antenna," JPL D-11853 and DSN 890-261 (internal document), Jet Propulsion Laboratory, Pasadena, California, August 28, 1997.

[15] "DSS-25 Ka-band Downlink Optics Delta Detail Technical Review," internal document, Jet Propulsion Laboratory, Pasadena, California, May 8, 1997.

[16] J. C. Chen, P. H. Stanton, and H. R. Reilly, Jr., "A Prototype Ka-/Ka-Band Dichroic Plate with Stepped Rectangular Apertures," *Telecommunications and Data Acquisition Progress Report 42-124*, vol. October–December 1995, http://tmo.jpl.nasa.gov/progress_report/issues.html Accessed October 2001.

[17] Y. H. Choung, K. R. Goudey, and L. G. Bryans, "Theory and Design of a Ku-Band TE21-Mode Coupler," *IEEE Transactions on Microwave Theory and Techniques*, vol. 30, no. 11, pp. 1862–1866, November 1982.

[18] M. A. Gudim, W. Gawronski, W. J. Hurd, P. R. Brown, and D. M. Strain, "Design and Performance of the Monopulse Pointing System of the DSN 34-Meter Beam-Waveguide Antennas," *Telecommunications and Mission Operations Progress Report 42-138*, vol. April–June 1999, http://tmo.jpl.nasa.gov/progress_report/issues.html Accessed October 2001.

[19] M. Franco and M. Britcliffe, "DSS-25 RF Performance Report," JPL Interoffice Memorandum 3336-97-003 (internal document), Jet Propulsion Laboratory, Pasadena, California, January 6, 1997.

[20] J. Prater, "System Noise Temperature Measurements of the Ka-band Feed at DSS-25," JPL Interoffice Memorandum 333-4-98-035 (internal document), Jet Propulsion Laboratory, Pasadena, California, August 4, 1998.

[21] K. Liewer, "A Problem with Two-Way Tracking at High Frequencies," JPL Interoffice Memorandum KML-91-66 (internal document), Jet Propulsion Laboratory, Pasadena, California, November 12, 1991.

[22] N. Rappaport, "Aberration Effects on Two-Way Tracking of a Spacecraft and Application to Cassini," JPL Interoffice Memorandum 312.F-97-037 (internal document) Jet Propulsion Laboratory, Pasadena, California, June 17, 1997.

[23] J. C. Chen, P. H. Stanton, and H. F. Reilly, "Performance of the X-/Ka-/KABLE-Band Dichroic Plate in the DSS-13 Beam-Waveguide Antenna," *Telecommunications and Data Acquisition Progress Report 42-115*, vol. July–September 1993, http://tmo.jpl.nasa.gov/progress_report/issues.html Accessed October 2001.

[24] P. H. Stanton, D. J. Hoppe, and H. Reilly, "Development of a 7.2-, 8.4-, and 32-Gigahertz (X-/X-/Ka-band) Three-Frequency Feed for the Deep Space Network," *Telecommunications and Mission Operations Progress Report 42-145*, vol. January–March 2001, http://tmo.jpl.nasa.gov/progress_report/issues.html Accessed October 2001.

[25] "Preliminary Design Review (PDR) BWG Ka-band Upgrades, internal document," Jet Propulsion Laboratory, Pasadena, California, February 8, 2000.